JOURNAL OF MATERIALS SCIENCE 25 (1990) 1203–1208

Compression creep of $Si_3N_4/MgAl_2O_4$ alloys

J. CRAMPON, R. DUCLOS, N. RAKOTOHARISOA
Laboratoire de Structure et Propriétés de l'Etat Solide, U.R.A. CNRS 790, Bât. C6, Université des Sciences et Techniques de Lille Flandres-Artois, 59655 Villeneuve d'Ascq Cedex, France

The compression creep behaviour in air of pressureless sintered $MgAl_2O_4$-doped Si_3N_4 was studied at temperatures between 1473 and 1593 K, and under stresses between 50 and 300 MPa. The variation of strain rate with stress and temperature was analysed to determine the stress exponent and the activation energy. Microstructural change was investigated by transmission electron microscopy. Up to 1533 K and 200 MPa (low temperature, low stress) viscous creep ($n \simeq 1$) appeared as the predominant mechanism of deformation. At 1593 K and 200 to 300 MPa (high temperature, high stress), extensive cavitation in intergranular vitreous phase produces the fracture of the samples. In the low-temperature region, strain whorls which are characteristic of grain-boundary sliding were observed at grain-boundaries in crept specimens.

1. Introduction

Si_3N_4-based ceramic alloys with the best high-temperature mechanical properties were fabricated recently by hot-pressure sintering. Today, ultrafine powders enable fully dense Si_3N_4 to be obtained via pressureless sintering. The pressureless sintering kinetics and hence final density of Si_3N_4 ceramics are improved by the use of a liquid sintering medium. It is now well known that, for Si_3N_4 alloys, the mechanical properties at high temperature are strongly affected by the residual vitreous phase located at triple junctions and grain boundaries [1–11]. As a result of this glassy film, and due to the degradation of mechanical properties at high temperature, substantial investigations have been directed at the analysis of the creep behaviour of Si_3N_4 in terms of the deformation mechanism by grain-boundary sliding and cavitation [1, 2, 4, 5, 7, 9, 11]. Depending on temperature, strain, stress, composition and/or microstructure (grain size, porosity, . . .) the grain-boundary sliding can be accommodated by a number of mechanisms for which models are known [12–17]. These include elastic strain at grain-boundary asperities, diffusional creep by direct material transport, viscous flow of glassy phase, dissolution precipitation of material, cavitational creep and plastic deformation by dislocation.

In view of the technological importance of Si_3N_4 alloys, a number of investigations have been undertaken of the mechanical behaviour in air of these materials, hot-pressed with different densification aids (MgO, Y_2O_3, Al_2O_3, AlN, . . .). Limited creep studies have been performed in environments other than air [1, 5, 11]. A programme of research, including the microstructural and mechanical study of creep in air or in a neutral atmosphere (nitrogen, argon) of pressureless-sintered $MgAl_2O_4$ and Y_2O_3/Al_2O_3-doped Si_3N_4, without and with TiN particles, has been started. The present paper is concerned with the results of creep experiments in air of the $MgAl_2O_4$-doped Si_3N_4 matrix, which are then compared with those for hot-pressed MgO-doped Si_3N_4.

2. Experimental procedure

2.1. Material

The $MgAl_2O_4$-doped Si_3N_4 was a commercial material supplied by the Ceramique Technique Desmarquest Laboratories, Trappes, France. Chemical analysis revealed that the major impurities in the starting Si_3N_4 powder were 1.8 wt % O, 0.46 wt % Fe, 0.27 wt % Al. Billets were prepared with high-purity $MgAl_2O_4$ powder, milled with WC balls, cold-pressed, and then pressureless-sintered in a nitrogen atmosphere. Crystalline phase identification by X-ray diffraction showed that the samples consisted of primarily β-Si_3N_4 with no detectable α-phase, and a very small quantity of WC phase.

All samples were examined by conventional transmission electron microscopy (TEM) throughout this study. Thin foils for TEM examination were taken from crept and from just heated samples. These foils were ion-thinned and then carbon coated to prevent charging in the microscope.

2.2. Creep testing

Specimens ($3 \times 3 \times 10\,mm^3$) were taken from pressureless-sintered billets. The three-point bending strength study made by the C.T.D. Laboratory at room temperature indicated that fracture stress was about 600 MPa for samples.

Samples density was determined before and after each test by hydrostatic weighing in pure alcohol. Before creep, specimen densities were found to be 3.04 and did not change significantly in unfractured crept specimens.

Compressional creep experiments were performed in air between 1473 and 1593 K, using a constant load machine. Stresses between 50 and 300 MPa were applied to the sample by alumina rods and silicon

0022–2461/90 $03.00 + .12

carbide discs to prevent indentation. Total dimensional variation was measured by an alumina probe which activated an LVDT, but whenever possible, the final dimensions of the sample were used to determine its strain. Load was applied only 1 h after temperature stabilization. The deformed samples were cooled down under load.

3. Results

3.1. Creep data

The relationship between apparent steady-state strain rate, stress and temperature was analysed with respect to the empirical law

$$\dot{\varepsilon} = A\sigma^n \exp \frac{-Q}{RT} \quad (1)$$

where the pre-exponential constant A was dependent on the microstructure (grain size, porosity, . . .) and composition of the sample.

The stress dependence of the creep rate (stress exponent n) was determined both by stress jumps on the same sample, or by comparing several samples at different stresses. The activation energy, Q, was obtained from temperature jumps. The stress exponent was measured at 1473, 1533 and 1593 K, while the activation energy was calculated between 1543 and 1593 K.

Typical creep curves, ε–t, are shown in Fig. 1 for samples deformed at 1533 K. A rather long period of transient creep was followed by an apparent steady state period. A final tertiary period with an acceleration of the creep strain up to fracture was observed at higher stress and temperature.

The stress exponent n ($\dot{\varepsilon} = A'\sigma^n$) was determined from the slope of the diagram log $\dot{\varepsilon}$ against log σ. Owing to the phenomenon of oxidation, the creep rates to this analysis were taken over the same period of the isothermal tests where nearly all samples exhibited quasi-steady creep rate. When specimen exhibited tertiary creep, the minimum creep rate value was used.

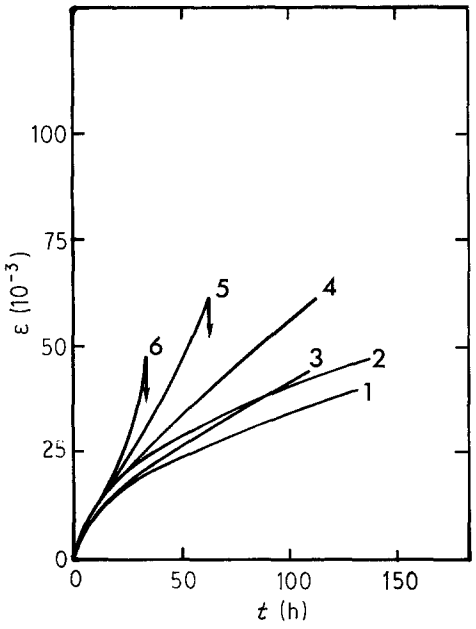

Figure 1 Creep curves ε–t at 1533 K (1260° C). (1) 50 MPa, (2) 70 MPa, (3) 100 MPa, (4) 140 MPa, (5) 200 MPa, (6) 300 MPa. Arrows indicate rupture of samples.

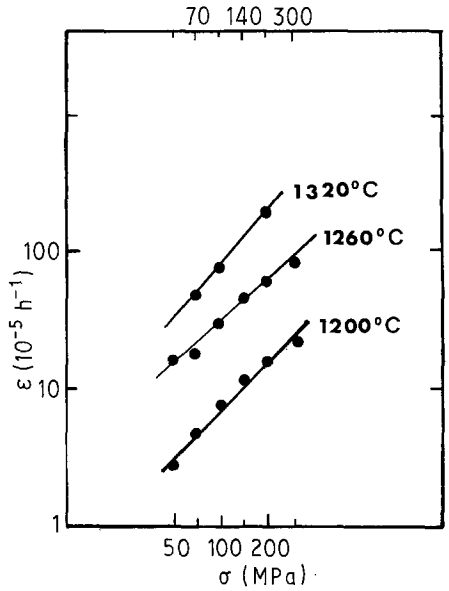

Figure 2 Strain-rate – stress relationships at 1473 K (1200° C), 1533 K (1260° C), 1593 K (1320° C).

Under these conditions, the stress exponent, n, was found to be 1.1 ± 0.1 (Fig. 2). The stress exponent was also determined by stress changes and was found to be ≃ 1. This agreement between the two determinations shows that isocomposition and isostructural conditions seem to be satisfied for the same test period at the same test temperature.

Isostructural activation energy from temperature jumps under a stress of 100 MPa, was found to be 600 kJ mol^{-1}.

3.2. Microstructural observations

All samples were examined by TEM in order to determine, at the grain level, how accommodation of the deformation was made between neighbouring grains. Specimen foils were taken from as-received, just heated, deformed and fractured samples.

Figure 3 is a typical transmission electron micrograph of as-received Si_3N_4. Initial microstructure is rather inhomogeneous, varying in form and grain size from regular hexagons of about 0.1 μm to elongated grains of about 1.5 μm. In most of the triple junctions, a residual glassy phase can be seen. In some cases, when it is thick, the intergranular glassy phase could be detected in conventional area diffraction by a diffuse halo as shown in Fig. 4.

Only heated, and deformed samples showed no significant change in their microstructure: submicrometre and micrometre grain size, intergranular glassy phase and very little evidence for dislocation activity within the grains.

The most distinctive additional feature found in deformed samples was strain-fringes, located along grain-boundaries. These strain whorls indicated the presence of localized internal stresses along grain boundaries. It was determined that no asperities could be resolved by conventional TEM at the centre of the whorls. In addition, only one single point per grain boundary appeared as the origin of the whorl contours (Fig. 5).

Samples which were deformed and fractured in the tertiary stage showed damaged areas where amorphous

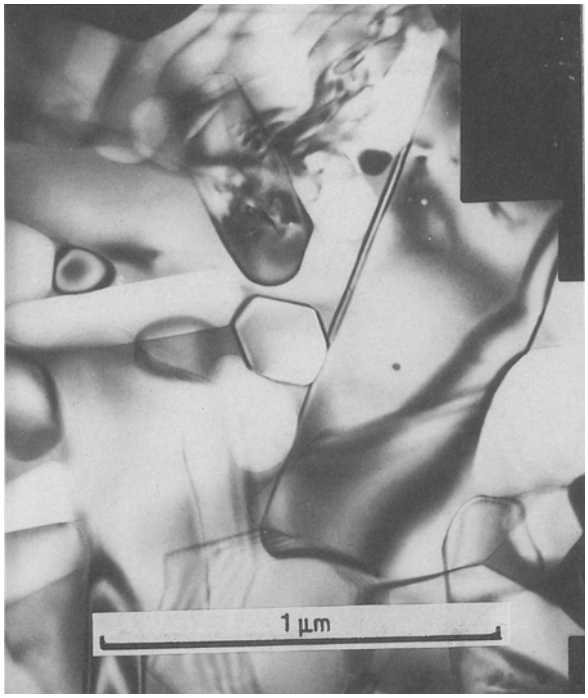

Figure 3 Transmission electron micrograph of as-received sample.

phase was prevalent. In these areas TEM revealed the appearance of pronounced cavitation. Spherical cavities at triple points and more elongated cavities extended at grain boundaries can be observed around the same grain (Fig. 6). In some cases, where the glassy phase was thick, several round-shaped cavities have been formed and grown within it (Fig. 7). In fractured samples, extended intergranular microcracks propagated along vitreous grain boundaries. Parallely, the growth of vitreous pockets at triple junctions was observed, which produced an intense diffuse halo in diffraction conditions (Fig. 8).

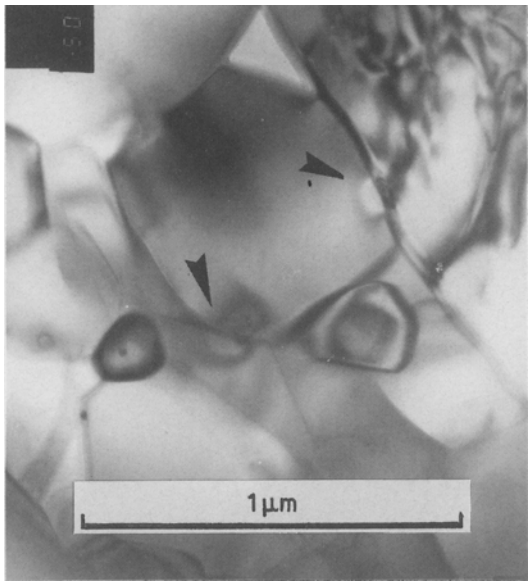

Figure 5 Transmission electron micrograph of crept sample showing strain whorls: $T = 1473$ K, $\sigma = 300$ MPa.

3.3. Oxidation phenomenon

After creep, external surfaces were covered with an opaque, and rather rough superficial film. Optical microscopy studies of cross-sections showed that the thickness of this scale was 40 μm after 162 h at 1533 K.

X-ray patterns of the external oxide phase at room temperature revealed the presence of $MgSiO_3$ and of a small amount of Mg_2SiO_4, formed together with α-SiO_2 and the vitreous film.

Concentration profiles through cross-section had been made for Al^{3+}, Mg^{2+} and Si^{4+} by secondary ion mass spectroscopy (SIMS) (IMS. 3F, CNRS, Meudon). The data were normalized with respect to silicon which showed a constant distribution over the whole

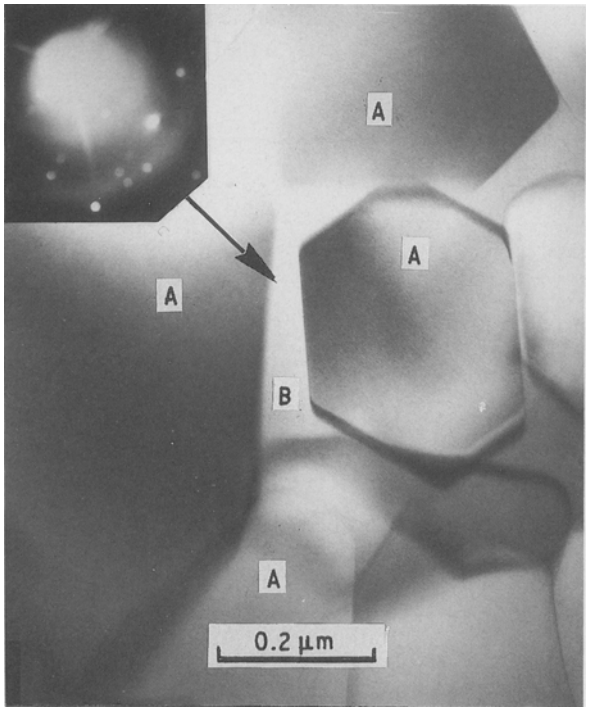

Figure 4 Transmission electron micrograph of as-received sample showing β-Si_3N_4 grains, A, and glassy phase, B.

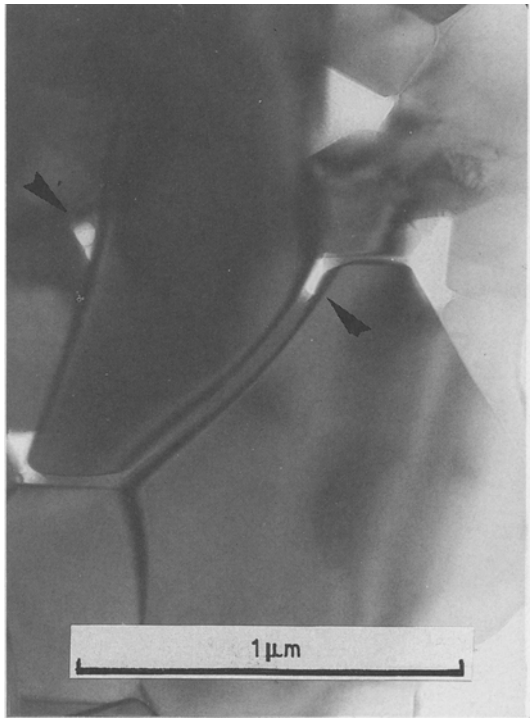

Figure 6 Transmission electron micrograph of fractured sample showing cavities at triple points and along grain boundaries: $T = 1533$ K, $\sigma = 300$ MPa.

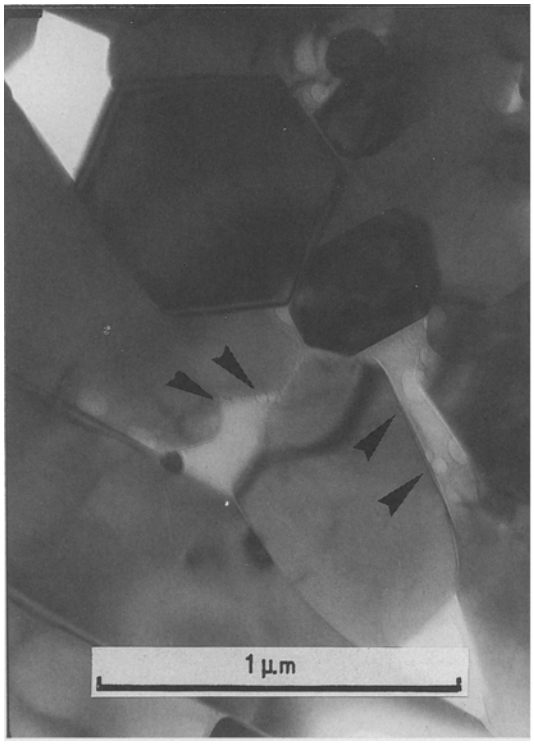

Figure 7 Transmission electron micrograph of fractured sample showing vapour bubbles within the glassy phase: $T = 1533\,K$, $\sigma = 300\,MPa$.

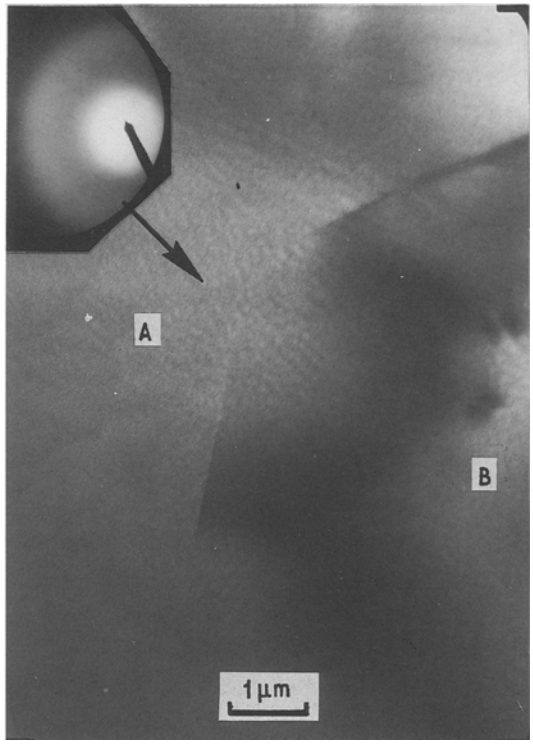

Figure 8 Transmission electron micrograph of fractured sample showing a large vitreous pocket, A, around a β-Si_3N_4 grain, B: $T = 1573\,K$, $\sigma = 200\,MPa$.

depth of all samples. The analysis did not show any migration of aluminium, but concentration profiles for magnesium revealed a depletion of this ion in a zone of 800 μm below the external oxide layer in specimen crept during 162 h at 1533 K (Fig. 9). This zone of internal reaction the colour of which was clearer than the bulk one, was also visible by the naked eye.

4. Discussion

4.1. Oxidation and microstructural features

The addition of $MgAl_2O_4$ for pressureless-sintering of Si_4N_4 produced simultaneous solid solution of Al^{3+} and O^{2-} ions in the lattice of β-Si_3N_4 to form a ceramic alloy of general composition $\beta'Si_{6-x}Al_xO_xN_{8-x}$ + glassy phase. Auger electron spectroscopy of the fracture surface provided evidence for grain-boundary segregation of Mg^{2+} in such $\beta'Si_3N_4$ ceramic alloys [3]. Here, the observed depletion of Mg^{2+} after creep will lie in the desegregation of these ions via their extraction into the superficial oxide scale to form $MgSiO_3$ and a small amount of Mg_2SiO_4. The Mg^{2+} ions which cannot be accommodated within the lattice of Si_3N_4 move during creep in air within the glassy phase, the composition of which has been shown to be nearly Mg_2SiO_4 for MgO-doped Si_3N_4 [11], and the observed oxidation is in agreement with the oxidation mechanism proposed by Clarke and Lange [18] for MgO-doped Si_3N_4.

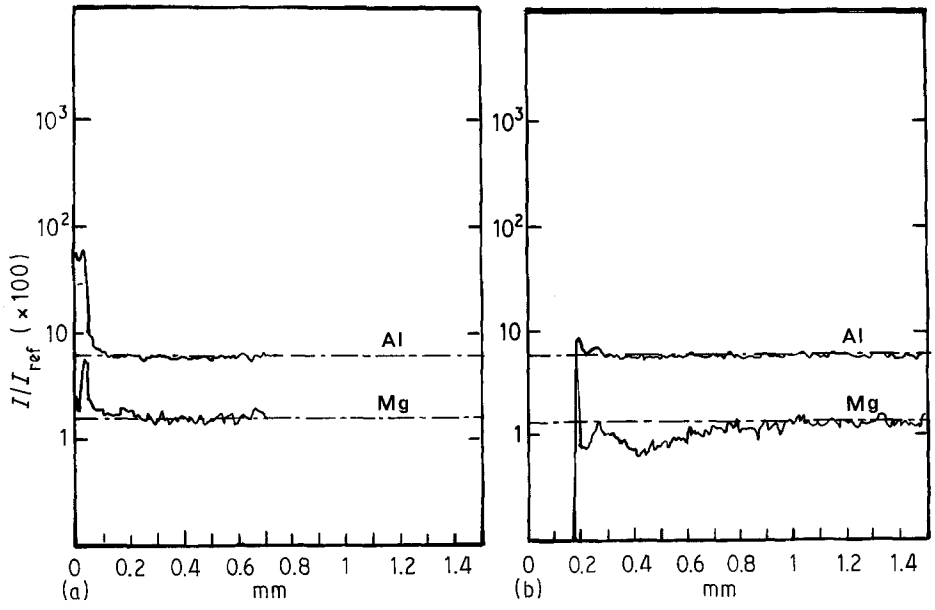

Figure 9 Concentration profiles for (a) reference sample and (b) crept sample.

The glassy phase was observed by TEM in as-received samples as small pockets at the multiple junctions, certainly interconnected by a very thin glassy layer at grain boundaries which was not detected here by conventional TEM.

During creep, this secondary phase remained amorphous and did not crystallize, The beneficial effect of oxidation by compositional change during creep [6] was not sufficient to prevent cavitation, at the highest stresses and temperatures, into the glassy interphase. Indeed, when temperature and stress reached limit values specimens failed by a ductile rupture occurring during a rather long state of accelerated creep. The mechanism of cavitation in tertiary creep seemed similar to other investigations on cavitational creep of Si_3N_4 and was not studied further.

4.2. Deformation mechanism during stationary creep

The dominant creep mechanism of $MgAl_2O_4$-doped Si_3N_4 can be determined from the preceding experimental data. The absence of dislocation substructure within the grains improves the predominance of deformation processes other than those involving dislocation movement. A similar conclusion has been drawn, for differently doped Si_3N_4, by several other investigators [1, 2, 6, 11].

The presence of strain whorls at the grain boundaries is the manifestation of a viscoelastic deformation by grain-boundary sliding which is prevalent during primary creep. After a transient state, the grain-boundary sliding has to be accommodated by some material transport in order to maintain the integrity of the sample.

As suggested by the value near unity found for the stress exponent, viscous creep must be the prevailing deformation mechanism in our pressureless sintered Si_3N_4. Owing to the presence of viscoelastic effects and glassy phase at grain-boundaries, pure diffusional creep processes [13–15] can be excluded in the present case. Indeed Coble creep, with a high activation energy ($820\,kJ\,mol^{-1}$) has only been observed by Karunaratne and Lewis [5] in hot-pressed low Mg-containing β'-Si_3N_4, with no detectable grain-boundary glassy phase. Moreover, grain-boundary sliding controlled by the viscous flow of glass from the boundary under compression to those under tension [3] can be ruled out, because the amount of vitreous phase between grain-boundaries in our materials was not sufficient to produce quasi-steady state deformation by this way. A stress exponent of 1, and strain whorls at stressed asperities form because of a mechanism where grain-boundary sliding is accommodated by material transport through the glassy phase [16].

In the present fine-grained Si_3N_4 with a vitreous interphase, grain-boundary sliding builds up stress singularities on adjacent boundaries and the asperities along boundaries act as stress concentrators and quickly develop a highly localized strain field. However it is in the transient state that the deformation proceeds mainly by a glide process which is driven by the stress distribution arising from the viscoelastic response of the polycrystal under load. When material transport is prevalent, the steady state stress distribution should come from the chemical potential gradient necessarily developed from the strain compatibility between neighbouring grains [19]. In this way the high normal stresses, which are generated after the relaxation of shear stresses, cause matter dissolution and redeposition in adjacent parts of the boundaries and most of the transient stress singularities should disappear. However, if numerous ledges are present on two adjacent grains, only one pair of ledges of opposing sign can lock together efficiently to act as a source of differential chemical potential. If a solution–precipitation mechanism eliminates this asperity, another pair of ledges should come into contact by further grain-boundary sliding. It is certainly the reason why only a single strain whorl per grain boundary was seen after steady-state creep.

This deformation process, which is in agreement with both our microstructural observations and the measured stress exponent of 1, is controlled by one of two steps acting in series, either by the transfer of atoms across the glass–Si_3N_4 crystal interface or by the diffusional transport through the glassy phase. If the rate-controlling step is the interface reaction, the activation energy will be bound to the activation energy for interface-controlled dissolution of β-Si_3N_4 crystal into the glass; if it is the diffusional transport of atoms through the glassy medium which is the limiting step, then the activation energy will depend on the viscosity of the glass.

The isostructural activation energy for creep found in the present work ($600\,kJ\,mol^{-1}$), agrees with that reported by other investigators for hot-pressed MgO-doped Si_3N_4 [1, 2, 4, 6]. Based on the Mg–Si–O–N system, and neglecting, for instance, the effect of aluminium, iron and other cation impurities, our material has an approximate composition Si_3N_4–SiO_2–MgO: 88–7.5–4.5 mol %, close to the Si_3N_4-Si_2N_2O tie line and far from the ternary eutectic in the Si_3N_4–Si_2N_2O–Mg_2SiO_4 compatibility triangle. Previous results of the-creep behaviour investigations of hot-pressed MgO-doped Si_3N_4 most remote from the ternary eutectic were dominated by a diffusional mechanism with $n = 1$, and a very low density of cavities [6]. Void formation during creep appeared qualitatively in our material similar to that observed in creep of hot-pressed MgO-doped Si_3N_4, although in our case cavitation was only visible in fractured samples. This indicates that in unfractured samples the void density was certainly too low to accommodate significantly the deformation. Thus, with regard to microscopic processes and not to creep resistance, the same deformation mechanism should be rate-controlling both for the present material and for material C in the previous work [6].

In the latter case, Tsai and Raj [20] believe that it is the interface-reaction step which is rate controlling. This conclusion has been drawn from the fact that the activation energy for interface-controlled dissolution rate of β-Si_3N_4 in an Mg–Si–O–N glass [21] can be of the order of the observed values for densification and creep rates [22]. Support for this view can be taken from the study of Hampshire and Jack [23] who have

concluded that the kinetic of sintering of MgO-doped Si_3N_4 is also interface-reaction controlled. Thus, if the viscosity of the glass phase does not increase drastically at the temperatures of the present work, it is allowable to think that the interface reaction is rate controlling in our case.

5. Conclusion

Compression creep tests in air have been made over a range of stresses at temperatures from 1473 to 1593 K on pressureless sintered $MgAl_2O_4$-doped Si_3N_4. In the investigated range, the stress and temperature dependence of the creep rate could be described by the equation

$$\dot{\varepsilon} = A\sigma^n \exp - \frac{Q}{RT}$$

with $n \simeq 1$ and $Q = 600\,\mathrm{kJ\,mol^{-1}}$.

Except for the highest temperature and stress values studied, cavitation was certainly too weak to accommodate significantly the deformation. Thus, the observed strain whorls show that grain-boundary sliding, facilitated by the glassy film, has to be accommodated by matter transport.

From microstructural observations, pure diffusional and viscous glass flow mechanisms can be ruled out. The solution–precipitation model is in better agreement with both the stress exponent and the presence of strain whorls.

The comparison of creep behaviour of $MgAl_2O_4$-doped Si_3N_4 and of hot-pressed MgO-doped Si_3N_4, allowed us to conclude that transfer of atoms across the glass–Si_3N_4 crystal interfaces is rate controlling and not the diffusion through the glass.

Acknowledgements

The authors thank Dr J. P. Torre *et al.*, C.T.D. Laboratories, for help in producing the material, and Drs P. Eveno and M. Schumacher for performing the IMS analysis. This work was supported by the French Research and Technology Ministry (M.R.T.).

References

1. R. KASSOWSKY, D. G. MILLER and R. S. DIAZ, *J. Mater. Sci.* **10** (1975) 983.
2. S. U. DIN and P. S. NICHOLSON, *ibid.* **10** (1975) 1375.
3. M. H. LEWIS, B. D. POWELL, P. DREW, R. J. LUMBY, B. NORTH and A. J. TAYLOR, *ibid.* **12** (1977) 61.
4. J. M. BIRCH and B. WILSHIRE, *ibid.* **13** (1978) 2627.
5. B. S. B. KARUNARATNE and M. H. LEWIS, *ibid.* **15** (1980) 449.
6. F. F. LANGE, B. I. DAVIS and D. R. CLARKE, *ibid.* **15** (1980) 601.
7. R. M. ARONS and J. K. TIEN, *ibid.* **15** (1980) 2046.
8. J. L. BESSON, A. BOUARROUDJ and P. GOURSAT, *Rev. Int. Hautes Temper. Refract. Fr.* **19** (1982) 381.
9. N. J. TIGHE, S. M. WIEDERHORN, J. J. CHUANG and C. L. McDANIEL, in "Deformation of Ceramic Materials II", edited by R. C. Bradt, Vol. 18 (1984) pp. 587–604.
10. A. BOUARROUDJ, P. GOURSAT and J. L. BESSON, *J. Mater. Sci.* **20** (1985) 1150.
11. M. BACKHAUSS-RICOULT, J. CASTAING and J. L. ROUTBORT, *Rev. Phys. Appl.* **23** (1988) 239.
12. R. RAJ and M. F. ASHBY, *Met. Trans.* **2** (1971) 1113.
13. F. R. N. NABARRO, "Deformation of Crystals by the Motion of Single Ions", in the Report on the Conference on Strength of Solids, Bristol, 7–8 July 1947 (The Physics Society, London, 1948) pp. 75–90.
14. C. HERRING, *J. Appl. Phys.* **21** (1950) 437.
15. R. L. COBLE, *ibid.* **34** (1963) 1679.
16. R. RAJ and C. K. CHYNG, *Acta Metall.* **29** (1981) 11, 159.
17. A. G. EVANS and A. RANA, *ibid.* **28** (1980) 129.
18. D. R. CLARKE and F. F. LANGE, *J. Amer. Ceram. Soc.* **63** (1980) 586.
19. J. R. SPINGARN and W. D. NIX, *Acta Metall.* **26** (1978) 1389.
20. R. L. TSAI and R. RAJ, *J. Amer. Ceram. Soc.* (1982) C 88.
21. *Idem, ibid.* **65** (1982) 270.
22. R. RAJ and P. E. D. MORGAN, *ibid.* (1981) C 143.
23. S. HAMPSHIRE and R. H. JACK, in "Progress in Nitrogen Ceramics", edited by Riley (1983) pp. 225–230.

Received 1 December 1988
and accepted 31 May 1989